nature neuroscience

ARTICLES

Tau promotes neurodegeneration through global chromatin relaxation

Bess Frost[1], Martin Hemberg[2], Jada Lewis[3] & Mel B Feany[1]

The microtubule-associated protein tau is involved in a number of neurodegenerative disorders, including Alzheimer's disease. Previous studies have linked oxidative stress and subsequent DNA damage to neuronal death in Alzheimer's disease and related tauopathies. Given that DNA damage can substantially alter chromatin structure, we examined epigenetic changes in tau-induced neurodegeneration. We found widespread loss of heterochromatin in tau transgenic *Drosophila* and mice and in human Alzheimer's disease. Notably, genetic rescue of tau-induced heterochromatin loss substantially reduced neurodegeneration in *Drosophila*. We identified oxidative stress and subsequent DNA damage as a mechanistic link between transgenic tau expression and heterochromatin relaxation, and found that heterochromatin loss permitted aberrant gene expression in tauopathies. Furthermore, large-scale analyses from the brains of individuals with Alzheimer's disease revealed a widespread transcriptional increase in genes that were heterochromatically silenced in controls. Our results establish heterochromatin loss as a toxic effector of tau-induced neurodegeneration and identify chromatin structure as a potential therapeutic target in Alzheimer's disease.

Tauopathies, including Alzheimer's disease, are characterized pathologically by the deposition of neurofibrillary tangles composed of the microtubule-associated protein tau in the brains of affected individuals[1]. The discovery of dominant mutations in the *tau* gene linked to a familial neurodegenerative disorder, frontotemporal dementia with parkinsonism linked to chromosome 17 (FTDP-17), confirms tau as a causal factor in neurodegenerative disease pathogenesis[2–4].

The precise mechanism of tau-induced neurotoxicity remains a critical question in tauopathy research, and understanding the molecular and cellular pathways perturbed by tau in disease states is essential for the development of effective therapies[5]. Although multiple lines of evidence implicate oxidative DNA damage and aberrant neuronal cell cycle activation in the toxic cascade triggered in tauopathies[6–8], the mechanisms controlling the interaction between these processes in terminally differentiated neurons are unknown. Based on recovery of chromatin regulators in unbiased forward genetic screens for modifiers of tau neurotoxicity[9,10] (M.B.F., unpublished data) and given the fact that chromatin remodeling is associated with oxidative DNA damage and cell cycle regulation[11,12], we hypothesized that oxidative stress–induced DNA damage causes chromatin alterations that promote cell cycle reentry in tauopathy.

An appropriate balance and distribution of active and repressed chromatin is required for proper transcriptional control, maintaining nuclear architecture and genomic stability[13], and regulating the cell cycle[14]. In the nucleus, DNA is packaged into specific chromatin domains known as euchromatin and heterochromatin. Euchromatin is generally gene rich and permissive for gene activation, whereas heterochromatin is relatively gene sparse and transcriptionally quiescent[12]. A set of highly conserved proteins and post-translational histone modifications maintain these distinct chromatin domains along chromosomes in both insects and vertebrates. In particular, dimethylated lysine 9 of histone 3 (H3K9me2) and the heterochromatin protein 1α (HP1α) are enriched in constitutive telomeric and pericentromeric heterochromatin[12]. Our results establish a role for H3K9me2, HP1α and heterochromatin loss in tau-mediated neurodegeneration in insect and vertebrate systems.

RESULTS

Heterochromatin loss in tau transgenic *Drosophila*

To explore an association between tau neurotoxicity and chromatin alterations, we first determined whether histone methylation patterns or chromatin-associated proteins are altered in the brains of tauopathy model *Drosophila*. Pan-neuronal transgenic expression of an FTDP-17 mutant form of human tau, tau^{R406W}, in *Drosophila* causes progressive neurodegeneration and provides a well-characterized *in vivo* genetic model of tau neurotoxicity[7,15,16]. We found that the total levels of H3K9me2 and HP1α were decreased in tau transgenic *Drosophila* heads compared with controls (**Fig. 1a**,**b**). Reverse transcription followed by PCR (RT-PCR) indicated that mRNA levels of *Su(var)3-9*, which encodes the main histone methyltransferase responsible for H3K9 dimethylation, and *Su(var)205*, which encodes HP1α, were equal between control and tau transgenic *Drosophila* heads, indicating that the loss of H3K9me2 and HP1α in tauopathy was not a result of transcriptional changes in these genes (**Supplementary Fig. 1a**). To determine whether heterochromatin loss is specific to tau^{R406W} versus a general feature of tau pathology, we used transgenic flies carrying human wild-type tau (tau^{WT})[15] or a pseudohyperphosphorylated form of human tau (tau^{E14})[7]. Tau phosphorylation is an important pathogenic event in Alzheimer's disease and related tauopathies, and the tau^{E14} transgene causes substantially more

[1]Department of Pathology, Brigham and Women's Hospital, Harvard Medical School, Boston, Massachusetts, USA. [2]Department of Ophthalmology and Program in Neurobiology, Boston Children's Hospital, Boston, Massachusetts, USA. [3]Department of Neuroscience and Center for Translational Research in Neurodegenerative Disease, University of Florida, Gainesville, Florida, USA. Correspondence should be addressed to M.B.F. (mel_feany@hms.harvard.edu).

Received 13 November 2013; accepted 24 December 2013; published online 26 January 2014; doi:10.1038/nn.3639

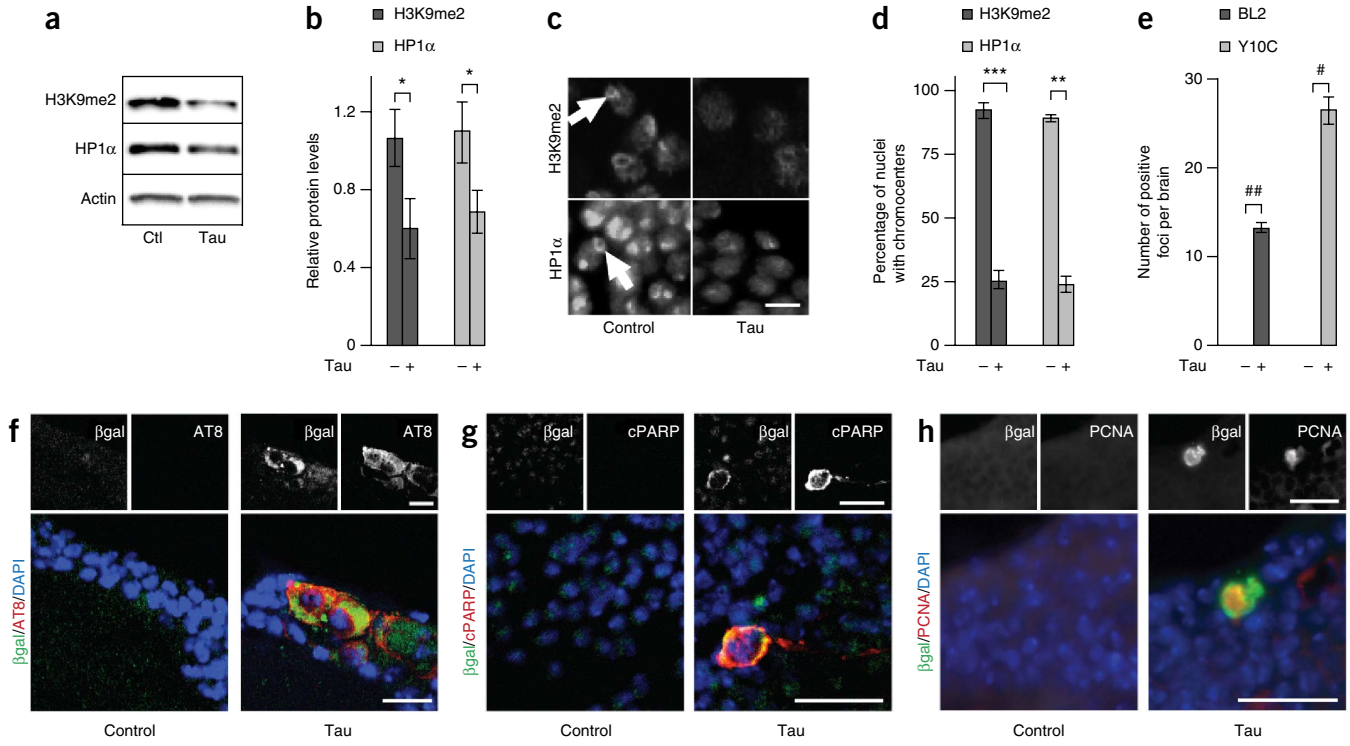

Figure 1 Tau transgenic *Drosophila* have widespread alterations in chromatin structure. (**a**) H3K9me2 and HP1α levels in control (Ctl) and tau transgenic fly head homogenates. The full-length blot is shown in **Supplementary Figure 5a**. (**b**) Quantification of **a** ($n = 5$ flies; for H3K9me2, $t = 3.14$; for HP1α, $t = 3.08$ for four degrees of freedom; $^{*}P = 0.04$, unpaired t test). (**c**) H3K9me2 and HP1α immunostaining of tau transgenic fly brains. Arrows indicate chromocenters. The region presented is cortex. Scale bar represents 3 μm. (**d**) Quantification of experiments in **c** ($n = 3$ brains; for H3K9me2, $^{***}P = 9 \times 10^{-5}$, $t = 105.36$ for two degrees of freedom, for HP1α, $^{**}P = 4.7 \times 10^{-5}$, $t = 145.24$ for two degrees of freedom; unpaired t test). Control is *elav-GAL4/+* in **a**–**d**. (**e**) Quantification BL2 (β-galactosidase) and Y10C (GFP) chromatin reporter activation in control and tau transgenic flies. Controls are *elav-GAL4/BL2* and *elav-GAL4/Y10C* ($n = 6$ brains; for BL2, $^{\#\#}P = 5.12 \times 10^{-9}$, $t = 81.94$ for five degrees of freedom; for HP1α, $^{\#}P = 1.13 \times 10^{-5}$, $t = 17.47$ for five degrees of freedom; unpaired t test). (**f**–**h**) β-galactosidase and AT8 (**f**) cleaved PARP (cPARP) (**g**) or PCNA (**h**) immunostaining in flies transgenic for the BL2 chromatin reporter ($n = 3$ brains). Control is *elav-GAL4/BL2* in **f** and **h**, and *elav-GAL4/BL2; UAS-PARP/+* in **g**. Scale bars represent 10 μm. Data are presented as mean ± s.e.m.; all flies are 10 d old.

toxicity in *Drosophila* than tau^{WT} or tau^{R406W} (refs. 7,16–18). Neuronal expression of tau^{WT} or tau^{E14} reduced H3K9me2 and HP1α levels (**Supplementary Fig. 1b**,**c**), indicating that heterochromatin defects are a general feature of tau-induced toxicity and are downstream of aberrant tau phosphorylation. The extent of heterochromatin loss caused by expression of tau^{WT} or tau^{E14} correlated with their respective toxicities. Given that expression of tau^{R406W} provides a level of toxicity that is well suited for genetic manipulation and biochemical analysis, tau^{R406W} was used primarily in our subsequent experiments, and we refer to it as tau hereafter for simplicity. To visualize heterochromatin structure directly, we stained control and tau transgenic brain sections with antibodies recognizing either H3K9me2 or HP1α. Nuclei of control brains contained prominent H3K9me2- and HP1α-rich heterochromatic foci, termed chromocenters. Tau transgenic *Drosophila*, however, had reduced chromocenter labeling, and instead had diffusely distributed H3K9me2 and HP1α (**Fig. 1c**,**d** and **Supplementary Fig. 1d**).

The highly condensed packaging of heterochromatic DNA renders it less accessible to polymerases and transcription factors, and genes embedded in heterochromatin are generally less highly transcribed than genes located in euchromatin. To determine whether chromatin relaxation permits expression of genes normally silenced by heterochromatin, we used transgenic *Drosophila* lines transgenic for either *LacZ* (BL2 reporter[19]) or *GFP* (Y10C reporter[20]) embedded in and silenced by heterochromatin. These reporters were silenced in controls, but were expressed in tau transgenic *Drosophila* brains (**Fig. 1e**). Transgenic expression of tau^{WT} or tau^{E14} also activated reporter expression in *Drosophila* (**Supplementary Fig. 1e**). 80% of β-galactosidase–positive foci in tau transgenic *Drosophila* were also positive for a disease-associated tau phosphoepitope (AT8; **Fig. 1f**) and 70% of β-galactosidase–positive foci were positive for cleaved PARP, a marker of caspase activation[21] (**Fig. 1g**). A number of studies in this model of tauopathy have demonstrated that reentry of postmitotic neurons into the cell cycle is a mechanism by which tau promotes neurotoxicity[7,8,16]. Accordingly, we found that 60% of β-galactosidase–positive foci in tau transgenic *Drosophila* were also positive for proliferating cell nuclear antigen (PCNA; **Fig. 1h**), an S phase marker of cell cycle activation. Together, these findings suggest that tau-induced heterochromatin loss permits aberrant gene expression that is coincident with tau neurotoxicity, cell cycle reentry and subsequent apoptosis of postmitotic neurons.

Genetic manipulation of chromatin modifies tau toxicity

To determine whether heterochromatin loss directly mediates cell death in our tauopathy model, we first asked whether restoring heterochromatin suppresses tau-induced toxicity. We stimulated heterochromatin formation in tau transgenic *Drosophila* by genetically manipulating genes that promote euchromatin. Ash1 is a histone methyltransferase that promotes euchromatin formation and transcriptional activation by methylating histones such as H3K4 and

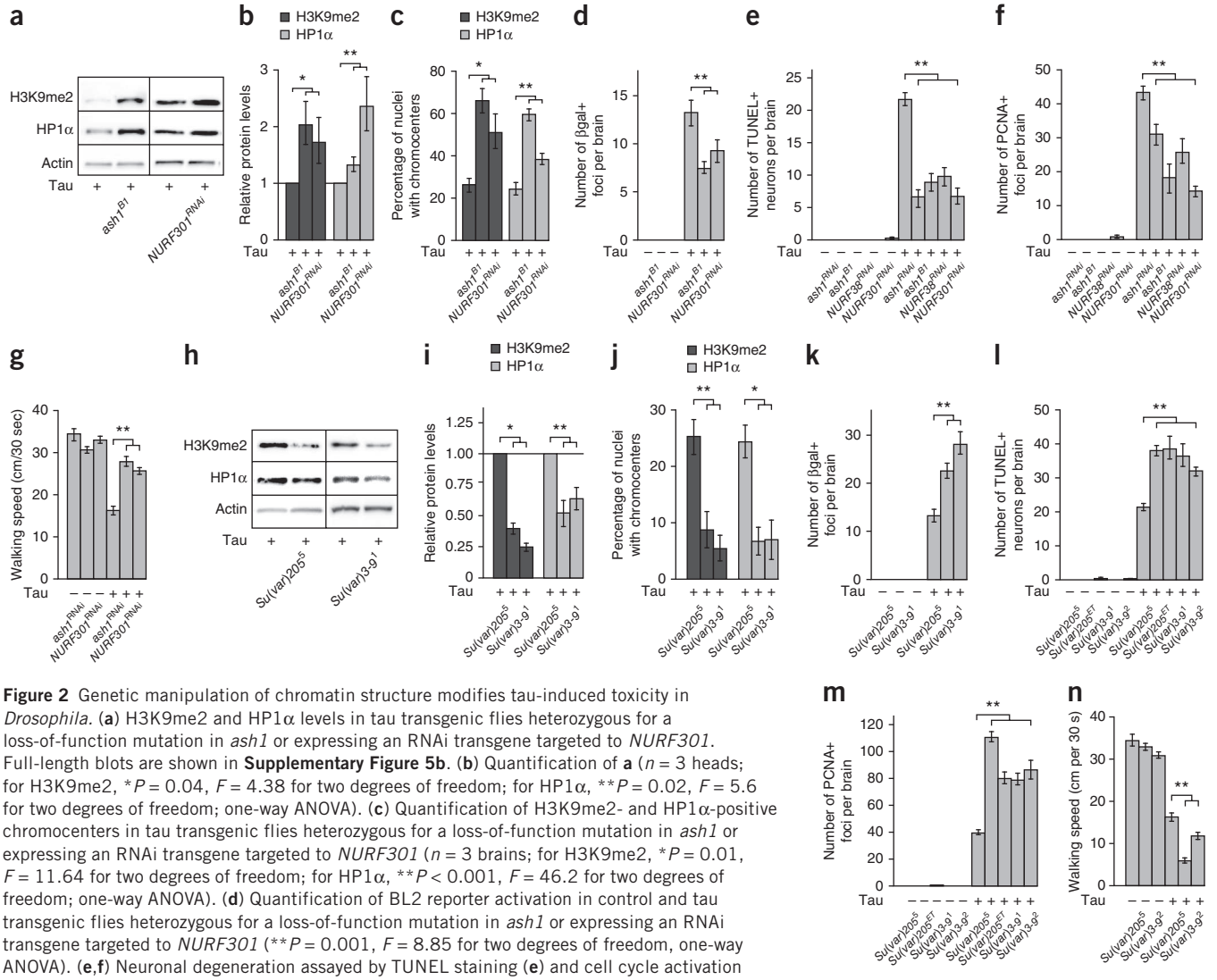

Figure 2 Genetic manipulation of chromatin structure modifies tau-induced toxicity in *Drosophila*. (**a**) H3K9me2 and HP1α levels in tau transgenic flies heterozygous for a loss-of-function mutation in *ash1* or expressing an RNAi transgene targeted to *NURF301*. Full-length blots are shown in **Supplementary Figure 5b**. (**b**) Quantification of **a** ($n = 3$ heads; for H3K9me2, $^{*}P = 0.04$, $F = 4.38$ for two degrees of freedom; for HP1α, $^{**}P = 0.02$, $F = 5.6$ for two degrees of freedom; one-way ANOVA). (**c**) Quantification of H3K9me2- and HP1α-positive chromocenters in tau transgenic flies heterozygous for a loss-of-function mutation in *ash1* or expressing an RNAi transgene targeted to *NURF301* ($n = 3$ brains; for H3K9me2, $^{*}P = 0.01$, $F = 11.64$ for two degrees of freedom; for HP1α, $^{**}P < 0.001$, $F = 46.2$ for two degrees of freedom; one-way ANOVA). (**d**) Quantification of BL2 reporter activation in control and tau transgenic flies heterozygous for a loss-of-function mutation in *ash1* or expressing an RNAi transgene targeted to *NURF301* ($^{**}P = 0.001$, $F = 8.85$ for two degrees of freedom, one-way ANOVA). (**e**,**f**) Neuronal degeneration assayed by TUNEL staining (**e**) and cell cycle activation assayed by PCNA staining (**f**) in brains of control and tau transgenic flies heterozygous for a loss-of-function mutation in *ash1* or expressing an RNAi transgene targeted to *ash1*, *NURF301* or *NURF38* (for TUNEL, $^{**}P < 0.001$, $F = 22.1$ for two degrees of freedom; for PCNA, $^{**}P < 0.001$, $F = 14.569$ for two degrees of freedom; one-way ANOVA). (**g**) Locomotor activity in control and tau transgenic flies expressing an RNAi transgene targeted to *ash1* or *NURF301* ($n = 18$ flies, $^{**}P < 0.001$, $F = 11.66$ with two degrees of freedom, one-way ANOVA). (**h**) H3K9me2 and HP1α levels in homogenates from heads of tau transgenic flies heterozygous for loss-of-function mutations in *Su(var)205* or *Su(var)3-9*. Full-length blots are shown in **Supplementary Figure 5c**. (**i**) Quantification of **h** ($n = 3$ heads; for H3K9me2, $^{*}P = 0.0002$, $F = 1{,}080.2$ for two degrees of freedom; for HP1α, $^{**}P = 0.01$, $F = 16.83$ for two degrees of freedom; one-way ANOVA). (**j**) Quantification of H3K9me2- and HP1α-positive chromocenters in tau transgenic flies heterozygous for a loss-of-function mutation in *Su(var)205* or *Su(var)3-9* based on immunofluorescence ($n = 3$ brains; for H3K9me2, $^{**}P = 0.01$, $F = 13.16$ for two degrees of freedom; for HP1α, $^{*}P = 0.02$, $F = 8.964$ for two degrees of freedom; one-way ANOVA). (**k**) Quantification of BL2 reporter activation in control and tau transgenic flies heterozygous for loss-of-function mutations in *Su(var)205* or *Su(var)3-9* ($^{**}P < 0.001$, $F = 21.2$ for two degrees of freedom, one-way ANOVA). (**l**,**m**) Neuronal apoptosis (**l**) and PCNA-positive foci (**m**) in control and tau transgenic flies heterozygous for loss-of-function mutations in *Su(var)205* or *Su(var)3-9* (for TUNEL, $^{**}P < 0.001$, $F = 10.26$ for four degrees of freedom; for PCNA, $^{**}P < 0.001$, $F = 34.48$ for four degrees of freedom; one-way ANOVA). (**n**) Locomotor activity in control and tau transgenic flies heterozygous for a loss-of-function mutation in *Su(var)205* or *Su(var)3-9* ($n = 18$ flies, $^{**}P < 0.001$, $F = 12.84$ for two degrees of freedom, one-way ANOVA). Flies were 10 d old and $n = 6$ unless otherwise specified. Controls are *elav-GAL4/+*. Data are presented as mean ± s.e.m.

H3K36 (ref. 22). The nucleosome remodeling factor (NURF) complex catalyzes ATP-dependent nucleosome sliding and is required for transcriptional activation[23]. In the context of transgenic tau expression, loss of ash1 or NURF complex function increased heterochromatin based on several assays. Total H3K9me2 and HP1α levels (**Fig. 2a**,**b** and **Supplementary Fig. 1f**,**g**) and H3K9me2 and HP1α chromocenter labeling (**Fig. 2c**) were increased in tau transgenic flies harboring a loss of function mutation in *ash1* or RNAi targeted to *NURF301*. Furthermore, loss of ash1 function or RNAi-mediated reduction of *NURF301* silenced expression of the heterochromatin-embedded reporter in tau transgenic flies (**Fig. 2d**). We found that genetically restoring heterochromatin in tau transgenic flies suppressed neuronal apoptosis (**Fig. 2e**) and reduced the number of PCNA-positive foci (**Fig. 2f**) by approximately 50%, directly implicating heterochromatin loss as a cause of cell cycle activation and neuronal death in tauopathy. RNAi transgenes targeted to *ash1*, *NURF301* and *NURF38* were not toxic in the absence of tau, nor was the loss of ash1 function. To assess the overall health of tau transgenic *Drosophila* in which

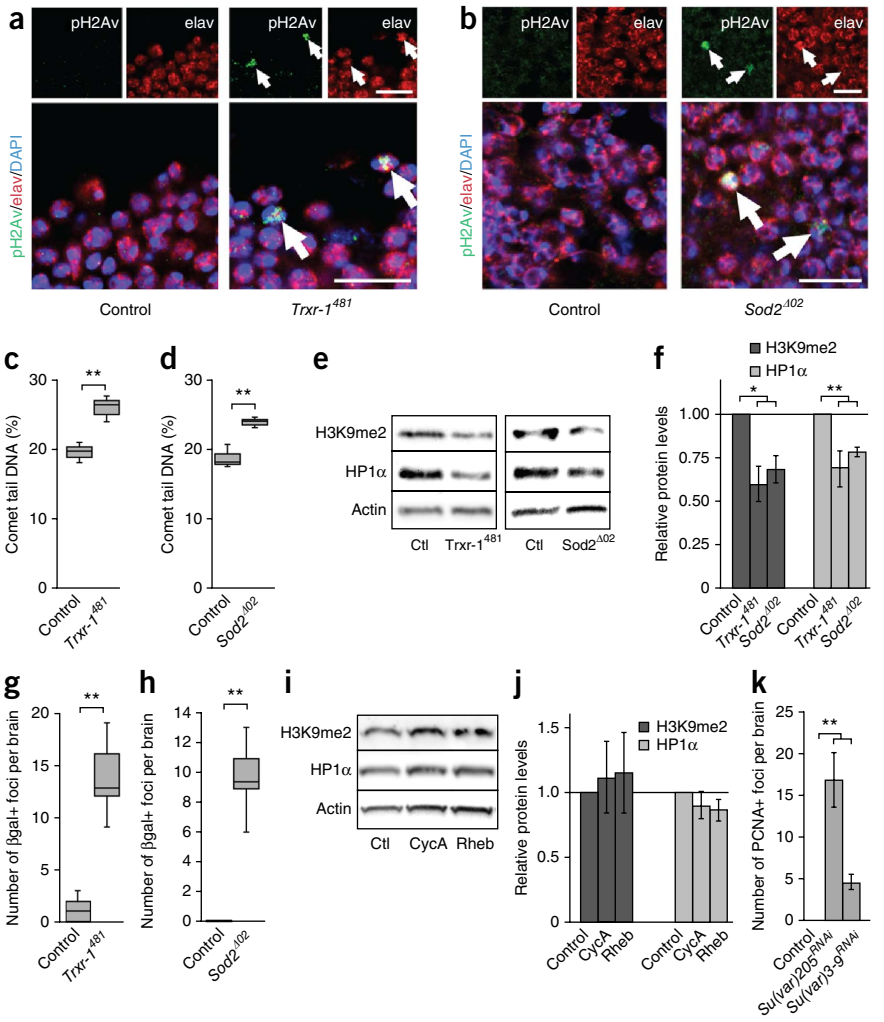

Figure 3 Oxidative stress causes DNA damage and heterochromatin loss in *Drosophila*. (**a**,**b**) pH2Av and elav staining in neurons of control and *Trxr-1*^{481} hemizygous (**a**) or *Sod2*$^{\Delta 02}$ heterozygous (**b**) mutant flies ($n = 3$ brains). Arrows indicate pH2Av positive nuclei. Scale bars represent 10 μm. (**c**,**d**) Quantification of comet tails in *Trxr-1*^{481} hemizygous (**c**) and *Sod2*$^{\Delta 02}$ heterozygous (**d**) mutant flies compared with control flies ($n = 6$ brains; $^{**}P = 0.01$, $t = 9.2$ for two degrees of freedom, **c**; $^{**}P = 0.01$, $t = 10.84$ for two degrees of freedom, **d**; unpaired t test). (**e**) H3K9me2 and HP1α levels in homogenates from heads of flies harboring loss-of-function mutations in *Trxr-1* or *Sod2*. Full-length blots are shown in **Supplementary Figure 5d**. (**f**) Quantification of experiments in **e** ($n = 3$ heads; for H3K9me2, $^{*}P = 0.02$, $F = 7.98$ for two degrees of freedom; for HP1α, $^{**}P = 0.03$, $F = 6.5$ for two degrees of freedom; one-way ANOVA). (**g**,**h**) Quantification of BL2 reporter activation in brains of *Trxr-1*^{481} (**g**) and *Sod2*$^{\Delta 02}$ (**h**) flies; control flies were hemizygous for the BL2 reporter ($n = 6$ brains; $^{**}P < 0.001$, $t = 20.19$ for five degrees of freedom, **g**; $^{**}P < 0.001$, $t = 26.56$ for five degrees of freedom, **h**; unpaired t test). (**i**) H3K9me2 and HP1α levels in homogenates from heads of flies with neuronal overexpression of CycA or Rheb. Full-length blots are shown in **Supplementary Figure 5e**. (**j**) Quantification of experiments in **i** ($n = 3$ heads; for H3K9me2, $P = 0.92$, $F = 0.08$ for two degrees of freedom; for HP1α, $P = 0.54$, $F = 0.71$ for two degrees of freedom; one-way ANOVA). (**k**) Cell cycle activation assayed by PCNA staining in brains of flies with RNAi-mediated knockdown of *Su(var)205* or *Su(var)3-9* ($n = 6$ brains, $^{**}P < 0.001$, $F = 23.52$ for two degrees of freedom, one-way ANOVA). Control flies were w^{1118} in **a**–**h** and *elav-GAL4/+* in **i**–**k**. *Trxr-1*^{481} hemizygous flies and respective controls were 2 d old, all other flies were 10 d old. Data are presented as mean ± s.e.m., except in **c**, **d**, **g** and **h** in which data are presented as box and whisker plots comprising minimum, lower quartile, median, upper quartile and maximum values.

heterochromatin is genetically restored, we measured the locomotor activity of control and transgenic flies. Tau transgenic *Drosophila* had reduced locomotor activity compared with control flies, and this locomotor deficit was rescued by RNAi-mediated reduction of *ash1* or *NURF301* (**Fig. 2g**). Tau transgenic *Drosophila* had similar mRNA levels of *ash1*, *NURF301* and *NURF38* compared with control flies, suggesting that tau did not cause heterochromatin changes by altering expression of these genetic modifiers (**Supplementary Fig. 1h**). We used RT-PCR to confirm knockdown of *ash1*, *NURF301* and *NURF38* mRNA levels in the heads of transgenic flies (**Supplementary Fig. 1i**).

We next determined whether further relaxation of heterochromatin enhances tau neurotoxicity. We reduced H3K9me2 and HP1α levels by expressing tau with heterozygous loss-of-function alleles of *Su(var)3-9* or *Su(var)205*. In the context of transgenic human tau, mutation of *Su(var)3-9* or *Su(var)205* further reduced H3K9me2 and HP1α levels (**Fig. 2h**,**i** and **Supplementary Fig. 1j**,**k**), caused additional loss of H3K9me2 and HP1α chromocenter labeling (**Fig. 2j**), and increased expression of the heterochromatin-embedded reporter (**Fig. 2k**) compared with expression of tau alone, indicating that these genetic manipulations exacerbate tau-induced heterochromatin loss. Tauopathy model flies harboring mutations in *Su(var)3-9* and *Su(var)205* had double the levels of neuronal apoptosis (**Fig. 2l**) and PCNA-positive foci (**Fig. 2m**) compared with the expression of tau alone. Notably, mutant *Su(var)3-9* and *Su(var)205* transgenes were not toxic in the absence of tau. Loss-of-function mutations in *Su(var)205* or *Su(var)3-9* also enhanced the locomotor deficits of tau transgenic *Drosophila* (**Fig. 2n**). In total, these genetic data imply that heterochromatin loss has a causal role in tau-induced neurotoxicity *in vivo*.

A major pathological feature of Alzheimer's disease and other tauopathies is the accumulation of abnormally phosphorylated forms of tau in the brains of affected individuals[1]. Genetically manipulating chromatin in the context of transgenic tau did not alter tau levels or the levels of the disease-associated tau phosphoepitopes PHF1, AT270 or AT8 (**Supplementary Fig. 1l**), despite modification of tau-induced toxicity. These results suggest that heterochromatin loss in tau transgenic *Drosophila* occurs downstream of tau phosphorylation and that suppression or enhancement of tau toxicity is not simply a result of altered tau expression.

Oxidative stress promotes DNA damage and heterochromatin loss

We next considered mechanisms whereby tau induces heterochromatin loss. Oxidative DNA damage and activation of the cell cycle are known to promote chromatin remodeling[11,12], are present in human

Alzheimer's disease brains[24,25] and are critical components of tau-induced neurodegeneration in our *Drosophila* model of tauopathy[7,8,16]. We first determined whether oxidative stress causes DNA damage and heterochromatin loss in *Drosophila*. We genetically induced oxidative stress in *Drosophila* using either a strong loss-of-function mutation in *Thioredoxin reductase-1* ($Trxr\text{-}1^{481}$)[26] or *Superoxide dismutase 2* ($Sod2^{\Delta 02}$)[27]. We have previously shown that loss of Trxr-1 or Sod2 function enhances tau neurotoxicity[16]. We assessed DNA damage in $Trxr\text{-}1^{481}$ and $Sod2^{\Delta 02}$ mutant flies on the basis of phosphorylation of Ser-139 of the histone variant H2Av (pH2Av), a marker of DNA double-strand breaks. Immunofluorescence revealed that pH2Av was present in the brains of $Trxr\text{-}1^{481}$ and $Sod2^{\Delta 02}$ mutant flies (**Fig. 3a**,**b**), but not in control flies. As a second measure of DNA damage, we performed the comet assay, which utilizes single-cell gel electrophoresis to quantify DNA single- and double-strand breaks. We observed an increase in the percent of DNA in comet tails in *Trxr-1* and *Sod2* mutant brains, confirming that these genetic manipulations damage DNA (**Fig. 3c**,**d**). Given that DNA damage can cause widespread heterochromatin loss[28,29] and reduced Trxr-1 or Sod2 function causes DNA damage, we asked whether loss of Trxr-1 or Sod2 function causes heterochromatin relaxation. Indeed, whole head homogenates from $Trxr\text{-}1^{481}$ and $Sod2^{\Delta 02}$ flies had reduced levels of H3K9me2 and HP1α (**Fig. 3e**,**f**) and increased activation of the heterochromatin-embedded reporter in the brain (**Fig. 3g**,**h**), supporting the idea that oxidative stress can cause heterochromatin loss in tauopathy.

Given that tau is known to aberrantly activate the cell cycle in neurons[7], we next determined whether neuronal cell cycle activation is upstream of heterochromatin loss. Neuronal overexpression of CycA or Rheb, two proteins known to promote the cell cycle, did not reduce H3K9me2 or HP1α levels (**Fig. 3i**,**j**) or activate the heterochromatin-embedded reporter (data not shown), suggesting that cell cycle activation does not cause widespread heterochromatin loss. Because cell cycle activation in postmitotic neurons causes apoptosis in *Drosophila*[7], these data also indicate that heterochromatin loss is not a result of general cellular toxicity. We next determined whether cell cycle activation occurs downstream of heterochromatin loss. Brains of *Drosophila* with RNAi-mediated neuronal knockdown of *Su(var)205* or *Su(var)3-9* were positive for PCNA (**Fig. 3k**), suggesting that heterochromatin loss is indeed upstream of aberrant cell cycle activation in neurons. We used RT-PCR to confirm RNAi-mediated knockdown of *Su(var)205* and *Su(var)3-9* (**Supplementary Fig. 2a**). Taken together, these data place oxidative stress–induced DNA damage upstream of heterochromatin loss in a sequence of cellular events that lead to aberrant cell cycle activation and subsequent neuronal apoptosis.

Tau-induced heterochromatin loss permits gene expression

To identify specific genes with reduced H3K9me2 levels, we performed H3K9me2-based ChIP-sequencing (ChIP-seq) in biological duplicate (**Fig. 4a**; http://genome.ucsc.edu)[30] and validated significantly H3K9me2-depleted genes with quantitative PCR (qPCR) (**Fig. 4b**). Given the known role of H3K9me2 in gene silencing, we expected that H3K9me2 loss at these loci would correlate with increased gene expression. Six of the genes (*Ago3*, *CG15115*, *CG15661*, *Ir41a*, *nvd* and *uif*) were upregulated in tau transgenic flies (**Fig. 4c**), as predicted. However, expression of the remaining five genes (*CG40006*, *Dscam*, *Gprk1*, *IntS3*, and *Snap25*) was unaffected by heterochromatin loss. These five genes were classified as moderately to highly expressed (modEncode Project[31]) in *Drosophila* heads despite their heterochromatic environment, whereas the six genes with increased expression in tau transgenic *Drosophila* were classified as heterochromatically silenced, with no to low baseline expression in *Drosophila* heads (**Fig. 4c**). These data suggest that baseline levels of gene transcription control how a gene embedded in heterochromatin will respond to heterochromatin loss. Thus, tau-induced heterochromatin loss only affects the expression of genes that are normally transcriptionally silenced by heterochromatin. Of the six genes that were both H3K9me2 depleted and transcribed at higher levels in tau transgenic *Drosophila*, two have human homologs. *Ago3* is homologous to the human gene *PIWIL1*, and *CG15661* is homologous to the human gene *UGT1A10*.

We next determined whether aberrant gene expression resulting from heterochromatin loss contributes substantially to tau-induced toxicity. As a proof of principle, we focused on *Ago3*, given its well-conserved human homolog and intriguing biological function. Ago3 regulates PIWI-associated RNAs (piRNAs)[32], a highly conserved class of small RNAs that are required for post-transcriptional gene silencing of transposons[33,34]. Consistent with increased transcription, Ago3 protein levels were increased by more than fourfold in tau transgenic *Drosophila* heads compared with control flies (**Fig. 4d**,**e**). To determine whether Ago3 overexpression directly contributes to tau neurotoxicity, we reduced *Ago3* levels in tau transgenic *Drosophila* using RNAi. We found fewer apoptotic and PCNA-positive cells in tau transgenic *Drosophila* brains expressing either of two nonoverlapping RNAi lines targeted to *Ago3* (**Fig. 4f**,**g**). RNAi mediated reduction of *Ago3* also suppressed the locomotor defects of tau transgenic *Drosophila* (**Fig. 4h**). Transgenic RNAi targeted to *Ago3* did not affect levels of transgenic tau or tau phosphorylation (**Supplementary Fig. 2b**), indicating that suppression of tau-induced toxicity was not a result of decreased tau expression or alterations in tau phosphorylation. RT-PCR confirmed RNAi-mediated knockdown of *Ago3* in the brains of transgenic flies (**Supplementary Fig. 2c**). These data strongly suggest that aberrant gene expression resulting from heterochromatin relaxation is a toxic mediator of tauopathy.

Heterochromatin loss in vertebrate tauopathies

Drosophila models of disease are valuable tools for generating and genetically testing hypotheses that can then be validated in higher organisms. We thus determined if heterochromatin loss is a conserved mechanism of tau-induced neurotoxicity. JNPL3 mice express human tau carrying the FTDP-17 mutation P301L (tau^{P301L}). These tau transgenic mice undergo progressive neurodegeneration and develop neurofibrillary tangles in the brain and spinal cord[35]. We investigated H3K9me2 and HP1α changes specifically in motor neurons, as they are a specifically vulnerable cell type in the JNPL3 model. In control mice, H3K9me2 and HP1α were concentrated in chromocenters at the nucleolar periphery. In tauopathy mice, however, ring-like perinucleolar chromocenter staining was reduced for both H3K9me2 and HP1α (**Fig. 5a–c**), similar to our observations in tau transgenic *Drosophila*. We next asked whether the aberrant expression of Ago3 present in tau transgenic *Drosophila* is conserved for its mammalian homolog, PIWIL1. Although PIWIL1 levels were very low in control mice, we observed approximately double the levels of PIWIL1 staining in motor neurons of tau transgenic mice (**Fig. 5d**). These data suggest that heterochromatin loss and aberrant gene expression are features of tauopathy that are conserved between *Drosophila* and mice.

The ultimate goal of our research is to identify mechanisms of tau-induced toxicity in human disease. Having observed heterochromatin loss and aberrant gene expression in *Drosophila* and mouse tauopathy models, we next investigated heterochromatin in Alzheimer's disease, the most common human tauopathy. We first used immunostaining to determine whether there are substantial differences in H3K9me2, HP1α and PIWIL1 expression between

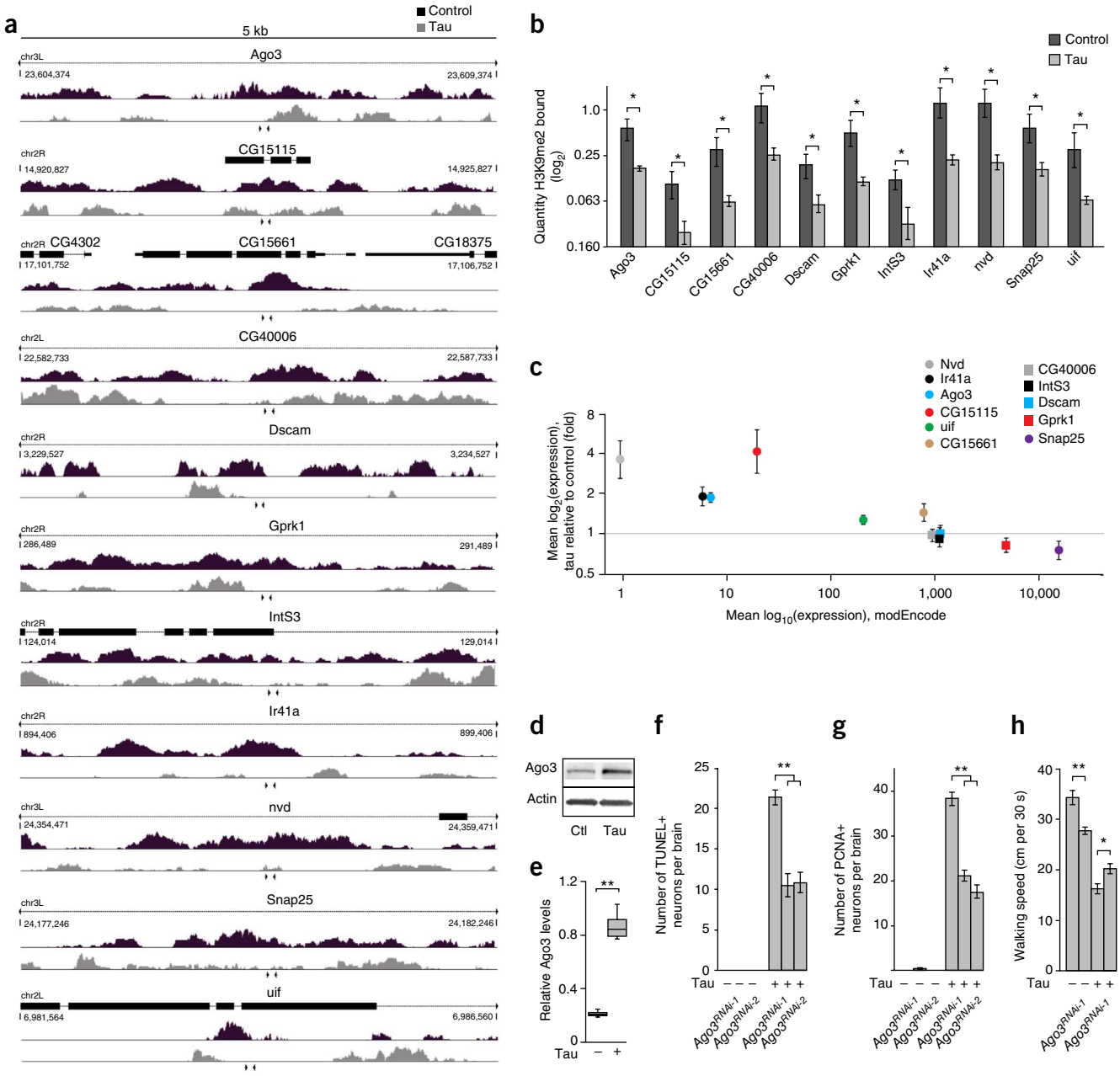

Figure 4 H3K9me2 loss and increased gene expression in tau transgenic *Drosophila*. (**a**) H3K9me2 distribution in genes with significant H3K9me2 loss in tau transgenic flies based on H3K9me2 ChIP-seq ($n = 2$ rounds of ChIP-seq on biological replicates, false discovery rate < 0.01). Arrows indicate the locations of primers used for qPCR. Rectangles indicate exons and dashed lines indicate introns. (**b**) qPCR of each gene identified by ChIP-seq as being H3K9me2 depleted in tau transgenic flies ($n = 3$ trials, 10 heads per trial; Ago3, $P = 0.02$, $t = 6.85$; CG15115, $P = 0.004$, $t = 15.6$; CG15661, $P = 0.01$, $t = 8.25$; CG40006, $P = 0.01$, $t = 9.56$; Dscam, $P = 0.0003$, $t = 54.42$; Gprk1, $P = 0.004$, $t = 15.07$; IntS3, $P = 0.0003$, $t = 62.71$; Ir41a, $P = 0.005$, $t = 14.38$; nvd, $P = 0.007$, $t = 12.31$; Snap25, $P = 0.004$, $t = 15.75$; uif, $P = 0.003$, $t = 19.15$; for two degrees of freedom, unpaired t test). $^{*}P < 0.05$. (**c**) Expression levels of H3K9me2-depleted genes in tau transgenic flies versus baseline gene expression (modEncode). Transcript levels are relative to both control and the endogenous control gene *RpL32* ($n = 3$ trials, 10 heads per trial, circles are significantly different ($P < 0.05$) from control, which is set to 1; Ago3, $P = 0.0003$, $t = 59.92$; CG15115, $P = 0.05$, $t = 4.33$; CG15661, $P = 0.04$, $t = 5.09$; CG40006, $P = 0.35$, $t = 1.2$; Dscam, $P = 0.48$, $t = 0.86$; Gprk1, $P = 0.053$, $t = 4.15$; IntS3, $^{*}P = 0.38$, $t = 1.13$; Ir41a, $P = 0.01$, $t = 9.79$; nvd, $P = 0.04$, $t = 4.91$; Snap25, $P = 0.05$, $t = 4.5$; uif, $P = 0.02$, $t = 6.29$; for two degrees of freedom, unpaired t test). (**d**) Ago3 levels in homogenates from control and tau transgenic fly heads. Full-length blots are shown in **Supplementary Figure 5f**. (**e**) Quantification of **d** ($n = 5$ heads; $^{**}P = 3.57 \times 10^{-7}$, $t = 63.98$ for four degrees of freedom, unpaired t test). (**f**,**g**) Neuronal degeneration assayed by TUNEL staining (**f**) and cell cycle activation assayed by PCNA staining (**g**) in brains of control and tau transgenic flies with RNAi-mediated reduction of *Ago3* ($n = 6$ brains; TUNEL, $^{**}P < 0.001$, $F = 29.92$ for two degrees of freedom; PCNA, $^{**}P < 0.001$, $F = 57.67$ for two degrees of freedom; one-way ANOVA). (**h**) Locomotor activity in control and tau transgenic flies with RNAi-mediated reduction of *Ago3* ($n = 18$ flies; $\text{Ago3}^{\text{RNAi-1}}$ compared with control, $^{**}P = 4.8 \times 10^{-16}$, $t = 6.56$ for 17 degrees of freedom; tau + $\text{Ago3}^{\text{RNAi-2}}$ compared with tau expressed alone, $^{*}P = 0.001$, $t = 3.865$ for 17 degrees of freedom; unpaired t test). Control was *elav-GAL4/+*. Data are presented as mean ± s.e.m., unpaired t-test or ANOVA. All flies were 10 d old.

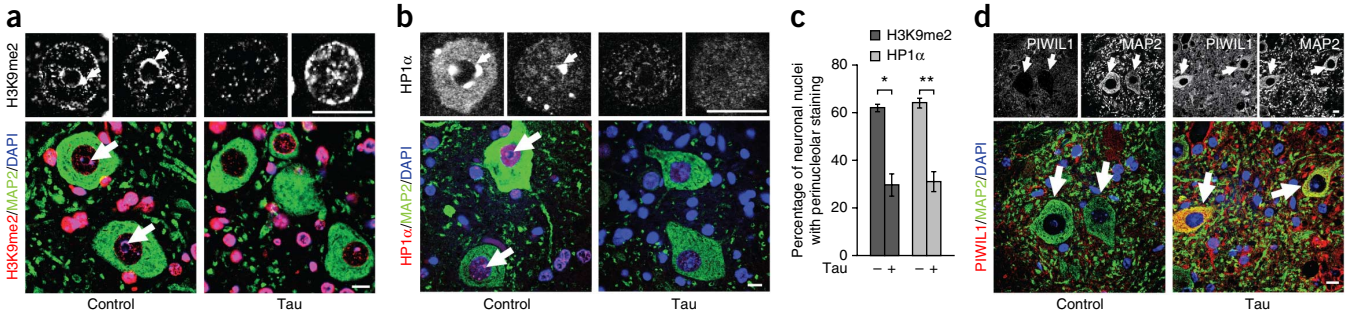

Figure 5 Tauopathy model mice have heterochromatin loss and increased PIWIL1 expression. (**a**,**b**) Perinucleolar chromocenter staining (arrows) of H3K9me2 (**a**) and HP1α (**b**) in control and JNPL3 motor neurons. Upper boxes show H3K9me2 or HP1α staining in MAP2-positive neurons at higher magnification. (**c**) Quantification of experiments shown in **a** and **b** (**a**, $*P = 0.002$, $t = 6.09$ for five degrees of freedom; **b**, $**P = 0.00002$, $t = 16.97$ for five degrees of freedom; unpaired t test). (**d**) PIWIL1 immunostaining (arrows) in control and JNPL3 motor neurons ($n = 6$ spinal cords per genotype). Scale bars represent 10 μm. Data are presented as mean ± s.e.m.

human control and Alzheimer's disease brains. In pyramidal hippocampal neurons from postmortem control brains, H3K9me2 was concentrated in perinucleolar chromocenters. In Alzheimer's disease brains, however, H3K9me2 staining was diffuse (**Fig. 6a**), similar to our observations in tau transgenic *Drosophila* and mice. For HP1α, diffuse staining was restricted to pyramidal neurons in Alzheimer's disease brains that were positive for the disease-associated tau phosphoepitope AT8, consistent with a link between tau toxicity and HP1α loss (**Supplementary Fig. 3a**). Immunofluorescence also revealed a widespread increase in PIWIL1 staining in hippocampal neurons from Alzheimer's disease brains (**Fig. 6b**). We next used quantitative methods to validate the loss of H3K9me2 and increase of PIWIL1 levels in Alzheimer's disease in age-, gender- and postmortem interval–matched cases and controls. Neurons outnumber glia ten to one in *Drosophila*[36]. In humans, however, the reverse is true, with glia being substantially more abundant than neurons. To eliminate the confounding effects of glia in humans, we purified nuclei from postmortem brain tissue and separated neuronal and glial nuclei via fluorescence

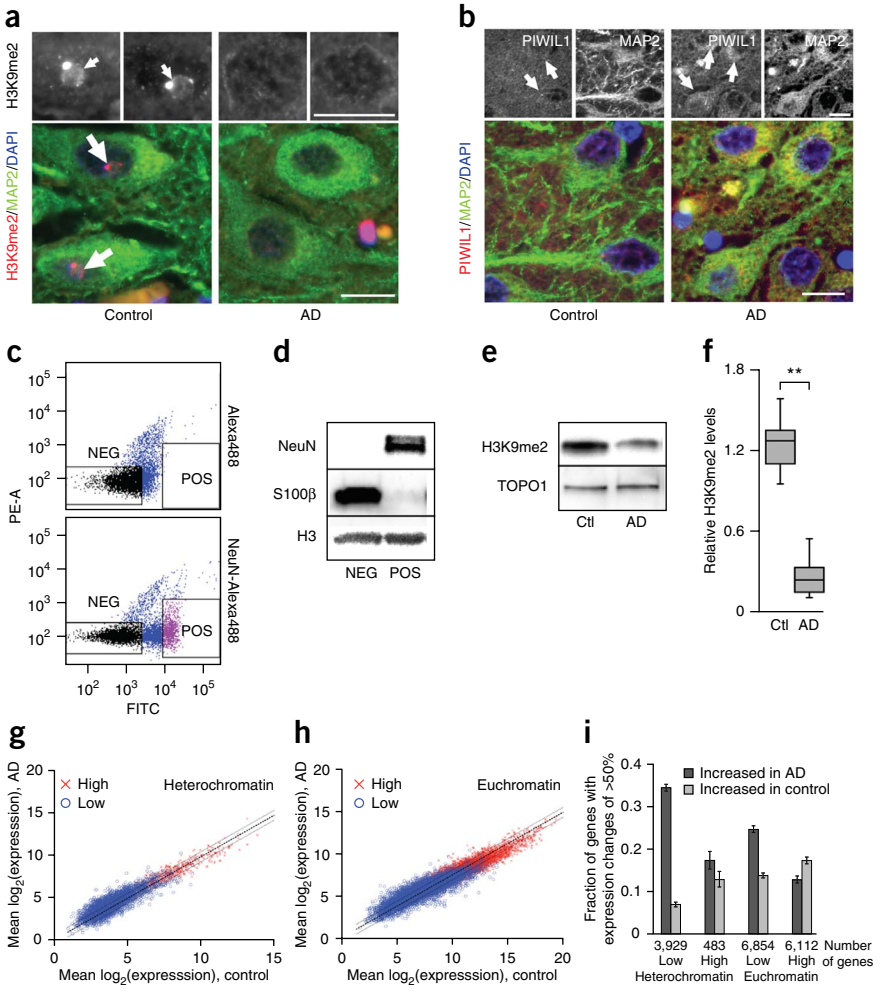

Figure 6 H3K9me2 loss and increased gene expression in human Alzheimer's disease brains. (**a**) Perinucleolar chromocenter staining of H3K9me2 (arrows) in human control and Alzheimer's disease (AD) hippocampal neurons ($n = 6$ brains). (**b**) PIWIL1 immunostaining (arrows) in control and human Alzheimer's disease hippocampal neurons ($n = 6$ brains). Upper boxes are H3K9me2 or PIWIL1 staining in MAP2-positive neurons at higher magnification in **a** and **b**. Scale bars represent 10 μm. (**c**) FACS of postmortem human cortical nuclei stained with the secondary antibody Alexa Fluor488 or the neuron-specific NeuN antibody and secondary antibody Alexa Fluor488. (**d**) S100β and NeuN levels in NeuN-negative (NEG) and NeuN-positive (POS) nuclear populations purified via FACS. Full-length blots are shown in **Supplementary Figure 5g**. (**e**) H3K9me2 levels in FACS-purified NeuN-positive neuronal nuclei from control and Alzheimer's disease brains. Full-length blots are shown in **Supplementary Figure 5h**. (**f**) Quantification of **e** ($n = 6$ brains; data are presented as box and whisker plots comprising minimum, lower quartile, median, upper quartile and maximum values for H3K9me2 levels, $**P = 0.00002$, $t = 15.95$ for two degrees of freedom, unpaired t-test). (**g**,**h**) Average mRNA levels of heterochromatic (**g**) and euchromatic (**h**) genes in laser-captured neurons from control ($n = 13$) and Alzheimer's disease ($n = 10$) postmortem hippocampi. Gray lines indicate a 50% gene expression threshold. (**i**) Bar plot of genes from **g** and **h** with expression changes greater than 50%. For increased expression of genes in Alzheimer's disease that are classified as heterochromatic and expressed at low levels in control, $P < 10^{-16}$, chi-squared test. Error bars in **i** reflect s.d. from 1,000 bootstraps.

activated cell sorting (FACS; **Fig. 6c**). Western blots with neuron-specific (NeuN) and astrocyte-specific (S100β) antibodies confirmed the purity of each nuclear population (**Fig. 6d**). We found that H3K9me2 was depleted in human Alzheimer's disease neurons (**Fig. 6e**,**f**). Similarly, RT-PCR of *PIWIL1* in FACS-purified neuronal nuclei revealed increased levels in human Alzheimer's disease neurons compared with controls. The geometric mean of *PIWIL1* levels relative to the endogenous control gene *CYC1* was 0.054 (s.e.m. = 0.022) in control brains and 0.216 (s.e.m. = 0.088) in Alzheimer's disease brains ($n = 6$ brains, $P < 0.05$ Wilcoxon rank-sum).

Having established that heterochromatin loss and PIWIL1 overexpression are conserved from our *Drosophila* model to human Alzheimer's disease, we took a global approach to determine whether heterochromatically silenced genes in human control brains are expressed at higher levels in Alzheimer's disease brains. On the basis of our findings in *Drosophila*, we predicted that heterochromatin loss in Alzheimer's disease permits the expression of genes that are heterochromatically silenced in control brains. Such changes most likely would not be detected in traditional analyses of gene expression because these analyses are often focused on genes with higher expression levels. To classify genes as heterochromatic or euchromatic, we used ChIP-seq data sets for all six publicly available histone modifications in the human hippocampus: H3K4me1, H3K4me3, H3K36me3, H3K9me3, H3K27me3 and H3K9ac (NIH Epigenomics Roadmap Project[37]). We used ChromHMM[38] (default settings) and data from these six histone modifications in the adult substantia nigra, midfrontal lobe, liver and fetal brain to define five different chromatin states (**Supplementary Fig. 3b**). On the basis of the presence of state three in known heterochromatic regions and the predominance of H3K9me3 and H3K27me3 in state four, we assigned states three and four as heterochromatic (**Supplementary Data Set 1**). To compare expression levels of heterochromatic and euchromatic genes between control and Alzheimer's disease brains, we used publicly available microarray data from laser-captured hippocampal neurons[39]. We used the present/absent detection call for each microarray probe to assign high or low gene expression for heterochromatic and euchromatic genes. We considered a gene to be highly expressed if it was called as present in at least 80% of the control and Alzheimer's disease samples. Notably, over one third of the genes that were heterochromatic and expressed at low levels in control hippocampal neurons were expressed at least 50% higher in Alzheimer's disease, including *PIWIL1* and *UGT1A10* (**Fig. 6g** and **Supplementary Data Set 2**), whereas only 13% of euchromatic genes with low expression were expressed at least 50% higher in Alzheimer's disease (**Fig. 6h**). The chi-square test indicated that the most significant transcriptional increase ($P < 10^{-16}$, chi-squared test) in Alzheimer's disease was for genes classified as heterochromatic and expressed at low levels in control (**Fig. 6i**). Large-scale gene expression changes were not observed in an unrelated liver disease (**Supplementary Fig. 3c**,**d**), suggesting that our results do not represent nonspecific effects of cellular toxicity.

Cellular differentiation is accompanied by a marked transition from a permissive chromatin state to a restrictive state that is rich in heterochromatin[40]. We hypothesized that heterochromatin relaxation in Alzheimer's disease causes a shift in gene expression back toward a dedifferentiated state. Indeed, the list of genes with increased expression in Alzheimer's disease reveals pluripotency-associated genes such as *POU1F1*, *NOG* and *NR5A2*. Pathway analysis using the PANTHER Classification System indicated that genes associated with developmental processes were significantly overrepresented ($P < 0.01$) in the list of genes that were heterochromatically silenced in controls and expressed at least 50% higher in Alzheimer's disease (**Supplementary Table 1**). We performed principal component analysis, a common technique for identifying patterns in complex data sets, to determine whether the gene expression profile in Alzheimer's disease has similarities to fetal brain. We compared gene expression profiles of fetal brains, human control hippocampal neurons, hippocampal neurons from Alzheimer's disease, and whole hippocampal tissue from controls and three stages of Alzheimer's disease. The first principal component that could not be trivially explained by different experimental conditions was the fourth, which assigned Alzheimer's disease hippocampal neurons, severe Alzheimer's disease hippocampi and fetal brains to the same principal component (**Supplementary Fig. 3e**). These analyses indicate that the expression profile of fetal brains is more similar to Alzheimer's disease hippocampi and hippocampal neurons than to control hippocampi or hippocampal neurons, consistent with a major global shift in gene expression in Alzheimer's disease toward a more fetal state.

Given that gene expression signatures in neurodegenerative diseases can be conserved from brain to peripheral tissues[41], we next compared expression levels of heterochromatic and euchromatic genes between control and Alzheimer's disease peripheral blood mononuclear cells (**Supplementary Fig. 3f**,**g**). Similar to Alzheimer's disease brain, 34.3% of genes that were heterochromatically silenced in control peripheral blood mononuclear cells were expressed at least 50% higher in cells from Alzheimer's disease samples (**Supplementary Data Set 3**), whereas only 17.0% of silenced genes in euchromatin were expressed at least 50% higher in Alzheimer's disease (**Supplementary Fig. 3h**), suggesting that changes in heterochromatin present in Alzheimer's disease brain are also present in peripheral blood.

DISCUSSION

We found that loss of normal heterochromatin promotes tau-mediated neurodegeneration *in vivo*. Our data, together with previous work from our laboratory and others, support a working model in which aberrant tau phosphorylation and/or aggregation is caused by amyloid-β[42], mutations in the *tau* gene[2–4], pathologic tau transfer[43] or as yet uncharacterized mechanisms. Pathologic tau causes an increase in actin stabilization[18] that inhibits association of the fission protein Drp1 with mitochondria, leading to mitochondrial elongation and the production of reactive oxygen species[44]. We found that oxidative stress causes DNA damage, heterochromatin loss and consequent aberrant gene expression in *Drosophila*. In cultured rat embryonic fibroblasts and in the adult rat liver, metabolic stress induced by caloric restriction increases Suv39h1, the mammalian homolog of Su(var)3-9 (ref. 45). These data raise the possibility that the stress and DNA damage control mechanisms differ in mitotic cells and postmitotic neurons. There is an extensive and evolving literature that documents mechanisms of DNA damage–induced chromatin relaxation, and we have previously implicated a number of proteins that regulate this process in the pathogenesis of tauopathy, including pH2Ax, ATM and p53 (ref. 8). Our data suggest that oxidative stress–induced DNA damage is one mechanism by which pathologic tau causes global heterochromatin relaxation; however, further work may reveal additional mechanisms of tau-induced heterochromatin loss. *In vitro* and in cultured cells, tau binds the minor groove of the DNA double helix and is thought to protect DNA from oxidative damage[46–48]. Our findings do not preclude a possible role for nuclear tau in the pathway of heterochromatin loss, as it is possible that tau dissociates from DNA and renders it more sensitive to reactive oxygen species caused by pathogenic tau in the cytoplasm. Our data suggest that DNA damage–induced heterochromatin loss causes a

global shift in gene expression toward a more developmental state that results from neuronal dedifferentiation, triggering inappropriate cell cycle reentry and subsequent apoptosis (**Supplementary Fig. 4**). Given that oxidative stress caused heterochromatin loss in our *Drosophila* tauopathy model, our findings raise the possibility that heterochromatin relaxation and subsequent aberrant gene expression are relevant to other neurodegenerative diseases that have been linked to oxidative stress.

Despite spatial obstacles, many genes embedded in heterochromatin are actively transcribed. Notably, we found that only those genes with no to low baseline levels of transcription in controls were upregulated in tau transgenic *Drosophila* and in human Alzheimer's disease. This observation may have implications for understanding chromatin biology, as it suggests that heterochromatically silenced genes are transcriptionally more sensitive than active genes to changes in the local chromatin environment. Although we focused our experiments on protein coding loci, heterochromatin loss likely permits increased expression of nonprotein-coding RNA transcripts. Indeed, increased expression of a regulatory RNA has already been implicated in the pathogenesis of Alzheimer's disease[49].

Heterochromatin loss and aberrant gene expression are conserved among *Drosophila*, mouse and human tauopathy, emphasizing the potential clinical relevance of these data. In a group of genes with substantial H3K9me2 loss in tau transgenic *Drosophila*, we focused specifically on *Ago3*, the *Drosophila* homolog of human *PIWIL1*. Ago3 regulates piRNAs, a large class of highly conserved, small, noncoding RNAs that are responsible for silencing transposons[33,34]. Genetic reduction of Ago3 suppressed tau neurotoxicity in *Drosophila*, and Ago3/PIWIL1 was overexpressed in tau transgenic *Drosophila* and mice and in human Alzheimer's disease. These data suggest that Ago3/PIWIL1-mediated piRNA biogenesis and subsequent transposable element control are deregulated in tauopathy. In addition, components of the piRNA pathway are associated with stem cell self-renewal and are aberrantly expressed in several types of somatic tumors[50], suggesting that dysregulation of the piRNA pathway leads to a loss of proliferative control. PIWIL1, and possibly other aberrantly transcribed coding and noncoding loci, represent previously unknown targets for therapeutic intervention in Alzheimer's disease. Furthermore, widespread changes in heterochromatic gene expression are conserved in the blood as well as the brain in patients with Alzheimer's disease, identifying a new class of candidate biomarkers.

METHODS

Methods and any associated references are available in the online version of the paper.

Accession codes. The raw sequence data obtained by ChIP-seq are available at NCBI GEO under series accession number GSE53719.

Note: Any Supplementary Information and Source Data files are available in the online version of the paper.

ACKNOWLEDGMENTS

A. Alekseyenko, N. Riddle and A. Minoda provided critical advice for the H3K9me2 ChIP experiments. J. Eissenberg (Saint Louis University School of Medicine), K. Maggert (Texas A&M University), J. Brennecke (Austrian Academy of Science) and F. Missirlis (National Polytechnic Institute) provided *Drosophila* stocks. We thank C. Lemere (Brigham and Women's Hospital), D. Borchelt and G. Xu (University of Florida) for generously providing important reagents. We performed confocal imaging at the Harvard NeuroDiscovery Center Enhanced Neuroimaging Core Facility. The TRiP at Harvard Medical School (NIH/HIGMS R01-GM084947) and the Vienna *Drosophila* RNAi Center provided transgenic RNAi fly stocks. Antibodies obtained from the Developmental Studies Hybridoma Bank were developed under the auspices of the National Institute of Child Health and Human Development and maintained by the University of Iowa. Antibodies obtained from the University of California Davis/US National Institutes of Health NeuroMab facility are supported by NIH grant U24NS050606 and maintained by the University of California Davis. This work was supported by a Ruth L. Kirschstein National Research Service Award F32AG039193 (B.F.), R01AG33518, a Senior Scholar Award from the Ellison Medical Foundation and a grant from the American Health Assistance Foundation/BrightFocus (M.B.F.), and US National Institutes of Health (1R21NS070250) and National Science Foundation grants (0954570) in support of M.H. Support was provided to J.L. through the University of Florida Department of Neuroscience.

AUTHOR CONTRIBUTIONS

B.F. and M.B.F. conceptualized the study. B.F. performed experiments and ChIP-seq analysis. M.H. performed human expression analysis, principal component analysis and provided guidance for ChIP-seq analysis. J.L. provided critical reagents and contributed to research design. B.F., M.B.F. and M.H. participated in interpreting data and wrote the manuscript. M.B.F. supervised the research.

COMPETING FINANCIAL INTERESTS

The authors declare no competing financial interests.

1. Lee, V.M., Goedert, M. & Trojanowski, J.Q. Neurodegenerative tauopathies. *Annu. Rev. Neurosci.* **24**, 1121–1159 (2001).
2. Hutton, M. *et al.* Association of missense and 5′-splice-site mutations in tau with the inherited dementia FTDP-17. *Nature* **393**, 702–705 (1998).
3. Poorkaj, P. *et al.* Tau is a candidate gene for chromosome 17 frontotemporal dementia. *Ann. Neurol.* **43**, 815–825 (1998).
4. Spillantini, M.G., Crowther, R.A., Kamphorst, W., Heutink, P. & van Swieten, J.C. Tau pathology in two Dutch families with mutations in the microtubule-binding region of tau. *Am. J. Pathol.* **153**, 1359–1363 (1998).
5. Holtzman, D.M., Mandelkow, E. & Selkoe, D.J. Alzheimer disease in 2020. *Cold Spring Harb. Perspect. Med.* **2**, a011585 (2012).
6. Kruman, I.I. *et al.* Cell cycle activation linked to neuronal cell death initiated by DNA damage. *Neuron* **41**, 549–561 (2004).
7. Khurana, V. *et al.* TOR-mediated cell-cycle activation causes neurodegeneration in a *Drosophila* tauopathy model. *Curr. Biol.* **16**, 230–241 (2006).
8. Khurana, V. *et al.* A neuroprotective role for the DNA damage checkpoint in tauopathy. *Aging Cell* **11**, 360–362 (2012).
9. Blard, O. *et al.* Cytoskeleton proteins are modulators of mutant tau-induced neurodegeneration in *Drosophila*. *Hum. Mol. Genet.* **16**, 555–566 (2007).
10. Ambegaokar, S.S. & Jackson, G.R. Functional genomic screen and network analysis reveal novel modifiers of tauopathy dissociated from tau phosphorylation. *Hum. Mol. Genet.* **20**, 4947–4977 (2011).
11. Smith, K.T. & Workman, J.L. Chromatin proteins: key responders to stress. *PLoS Biol.* **10**, e1001371 (2012).
12. Dillon, N. Heterochromatin structure and function. *Biol. Cell* **96**, 631–637 (2004).
13. Peng, J.C. & Karpen, G.H. Heterochromatic genome stability requires regulators of histone H3 K9 methylation. *PLoS Genet.* **5**, e1000435 (2009).
14. De Lucia, F., Ni, J.Q., Vaillant, C. & Sun, F.L. HP1 modulates the transcription of cell-cycle regulators in *Drosophila melanogaster*. *Nucleic Acids Res.* **33**, 2852–2858 (2005).
15. Wittmann, C.W. *et al.* Tauopathy in *Drosophila*: neurodegeneration without neurofibrillary tangles. *Science* **293**, 711–714 (2001).
16. Dias-Santagata, D., Fulga, T.A., Duttaroy, A. & Feany, M.B. Oxidative stress mediates tau-induced neurodegeneration in *Drosophila*. *J. Clin. Invest.* **117**, 236–245 (2007).
17. Steinhilb, M.L., Dias-Santagata, D., Fulga, T.A., Felch, D.L. & Feany, M.B. Tau phosphorylation sites work in concert to promote neurotoxicity *in vivo*. *Mol. Biol. Cell* **18**, 5060–5068 (2007).
18. Fulga, T.A. *et al.* Abnormal bundling and accumulation of F-actin mediates tau-induced neuronal degeneration *in vivo*. *Nat. Cell Biol.* **9**, 139–148 (2007).
19. Lu, B.Y., Ma, J. & Eissenberg, J.C. Developmental regulation of heterochromatin-mediated gene silencing in *Drosophila*. *Development* **125**, 2223–2234 (1998).
20. Paredes, S. & Maggert, K.A. Ribosomal DNA contributes to global chromatin regulation. *Proc. Natl. Acad. Sci. USA* **106**, 17829–17834 (2009).
21. Williams, D.W., Kondo, S., Krzyzanowska, A., Hiromi, Y. & Truman, J.W. Local caspase activity directs engulfment of dendrites during pruning. *Nat. Neurosci.* **9**, 1234–1236 (2006).
22. Beisel, C., Imhof, A., Greene, J., Kremmer, E. & Sauer, F. Histone methylation by the *Drosophila* epigenetic transcriptional regulator Ash1. *Nature* **419**, 857–862 (2002).

23. Tsukiyama, T. & Wu, C. Purification and properties of an ATP-dependent nucleosome remodeling factor. *Cell* **83**, 1011–1020 (1995).
24. Hensley, K. *et al.* Electrochemical analysis of protein nitrotyrosine and dityrosine in the Alzheimer brain indicates region-specific accumulation. *J. Neurosci.* **18**, 8126–8132 (1998).
25. Mullaart, E., Boerrigter, M.E., Ravid, R., Swaab, D.F. & Vijg, J. Increased levels of DNA breaks in cerebral cortex of Alzheimer's disease patients. *Neurobiol. Aging* **11**, 169–173 (1990).
26. Missirlis, F. *et al.* Mitochondrial and cytoplasmic thioredoxin reductase variants encoded by a single *Drosophila* gene are both essential for viability. *J. Biol. Chem.* **277**, 11521–11526 (2002).
27. Marygold, S.J. *et al.* FlyBase: improvements to the bibliography. *Nucleic Acids Res.* **41**, D751–D757 (2013).
28. Hittelman, W.N. & Pollard, M. Visualization of chromatin events associated with repair of ultraviolet light-induced damage by premature chromosome condensation. *Carcinogenesis* **5**, 1277–1285 (1984).
29. Rubbi, C.P. & Milner, J. p53 is a chromatin accessibility factor for nucleotide excision repair of DNA damage. *EMBO J.* **22**, 975–986 (2003).
30. Kent, W.J. *et al.* The human genome browser at UCSC. *Genome Res.* **12**, 996–1006 (2002).
31. Celniker, S.E. *et al.* Unlocking the secrets of the genome. *Nature* **459**, 927–930 (2009).
32. Brennecke, J. *et al.* Discrete small RNA-generating loci as master regulators of transposon activity in *Drosophila*. *Cell* **128**, 1089–1103 (2007).
33. Aravin, A. *et al.* A novel class of small RNAs bind to MILI protein in mouse testes. *Nature* **442**, 203–207 (2006).
34. Girard, A., Sachidanandam, R., Hannon, G.J. & Carmell, M.A. A germline-specific class of small RNAs binds mammalian Piwi proteins. *Nature* **442**, 199–202 (2006).
35. Lewis, J. *et al.* Neurofibrillary tangles, amyotrophy and progressive motor disturbance in mice expressing mutant (P301L) tau protein. *Nat. Genet.* **25**, 402–405 (2000).
36. Edwards, T.N. & Meinertzhagen, I.A. The functional organisation of glia in the adult brain of *Drosophila* and other insects. *Prog. Neurobiol.* **90**, 471–497 (2010).
37. Bernstein, B.E. *et al.* The NIH Roadmap Epigenomics Mapping Consortium. *Nat. Biotechnol.* **28**, 1045–1048 (2010).
38. Ernst, J. & Kellis, M. ChromHMM: automating chromatin-state discovery and characterization. *Nat. Methods* **9**, 215–216 (2012).
39. Blalock, E.M. *et al.* Incipient Alzheimer's disease: microarray correlation analyses reveal major transcriptional and tumor suppressor responses. *Proc. Natl. Acad. Sci. USA* **101**, 2173–2178 (2004).
40. Zhu, J. *et al.* Genome-wide chromatin state transitions associated with developmental and environmental cues. *Cell* **152**, 642–654 (2013).
41. Cooper-Knock, J. *et al.* Gene expression profiling in human neurodegenerative disease. *Nat. Rev. Neurol.* **8**, 518–530 (2012).
42. Ittner, L.M. & Gotz, J. Amyloid-beta and tau–a toxic pas de deux in Alzheimer's disease. *Nat. Rev. Neurosci.* **12**, 65–72 (2011).
43. Frost, B., Jacks, R.L. & Diamond, M.I. Propagation of tau misfolding from the outside to the inside of a cell. *J. Biol. Chem.* **284**, 12845–12852 (2009).
44. DuBoff, B., Gotz, J. & Feany, M.B. Tau promotes neurodegeneration via DRP1 mislocalization *in vivo*. *Neuron* **75**, 618–632 (2012).
45. Bosch-Presegué, L. *et al.* Stabilization of Suv39H1 by SirT1 is part of oxidative stress response and ensures genome protection. *Mol. Cell* **42**, 210–223 (2011).
46. Krylova, S.M. *et al.* Tau protein binds single-stranded DNA sequence specifically—the proof obtained *in vitro* with non-equilibrium capillary electrophoresis of equilibrium mixtures. *FEBS Lett.* **579**, 1371–1375 (2005).
47. Sjöberg, M.K., Shestakova, E., Mansuroglu, Z., Maccioni, R.B. & Bonnefoy, E. Tau protein binds to pericentromeric DNA: a putative role for nuclear tau in nucleolar organization. *J. Cell Sci.* **119**, 2025–2034 (2006).
48. Wei, Y. *et al.* Binding to the minor groove of the double-strand, tau protein prevents DNA from damage by peroxidation. *PLoS ONE* **3**, e2600 (2008).
49. Faghihi, M.A. *et al.* Expression of a noncoding RNA is elevated in Alzheimer's disease and drives rapid feed-forward regulation of beta-secretase. *Nat. Med.* **14**, 723–730 (2008).
50. Juliano, C., Wang, J. & Lin, H. Uniting germline and stem cells: the function of Piwi proteins and the piRNA pathway in diverse organisms. *Annu. Rev. Genet.* **45**, 447–469 (2011).

ONLINE METHODS

Genetics and animal models. *Drosophila melanogaster* crosses and aging were performed at 25 °C. Flies expressing tau^{R406W}, tau^{WT} and tau^{E14} have been described previously[7,15,16]. The pan-neuronal *elav-GAL4* driver was used to drive tau and RNAi transgene expression. The following *Drosophila* lines were obtained from the Bloomington *Drosophila* Stock Center: *Sod2$^{\Delta 02}$*, *ash1^{B1}*, *ash1^{JF01498}*, *NURF38^{JF01299}*, *NURF301^{JF01709}*, *Su(var)205^{5}*, *Su(var)205^{MB11439}*, *Su(var)3-9^{1}*, *Su(var)3-9^{2}*, *Ago3^{GL00117}* and *Ago3^{HMS00125}*. *Su(var)3-9* and *Su(var)205* RNAi lines were obtained from the Vienna *Drosophila* RNAi center (lines number 39377 and 31995). The following investigators kindly contributed fly stocks: BL2 chromatin reporter, J. Eissenberg; Y10C chromatin reporter, K. Maggert; *Trxr-1^{481}*, F. Missirlis; UAS-CycA, C. Lehner (University of Zurich); UAS-Rheb, P. Gallant (University of Zurich). JNPL3 mice (*Mus musculus*) were originally developed on a C57BL/DBA2/SW background. JNPL3 mice were housed 2–5 per cage in a vivarium with a 12-h off/on light/dark cycle and were used compliance with ethical guidelines and regulations. With the approval of the Institutional Animal Care and Use Committee at Mayo Clinic and University of Florida, these mice underwent non-invasive behavioral testing to assess motor function and disease progression, including: assessment of escape extension during tail elevation, the righting reflex when turned on their backs, and the ability to grasp and hang from a rope during rope hang tests. Spinal cords of 8.5–14-month-old JNPL3 tau transgenic mice (five males and one female) and nontransgenic control littermates were analyzed (three males and three females).

Immunostaining. Antibodies are summarized in **Supplementary Table 2**. Formalin-fixed, paraffin-embedded sections from *Drosophila* heads, mouse spinal cord or human brain were used for immunostaining experiments. Sodium citrate–based antigen retrieval was performed before staining. For cPARP, pH2Av and elav staining, *Drosophila* brains were dissected in phosphate-buffered saline and fixed in methanol for 20 min before staining. A commercially available kit was used for TUNEL staining (Calbiochem, TdT FragEL). β-galactosidase, TUNEL and PCNA-positive nuclei were counted throughout the entire brain. Secondary antibodies were fluorescent except in the case of H3K9me2 and HP1α staining in **Supplementary Figure 1d**, and quantification of β-galactosidase, TUNEL and PCNA, in which secondary detection was performed with DAB. Brains were imaged on a Nikon Eclipse E600 fluorescent microscope with SPOT software or a Zeiss LSM 510 META upright confocal microscope. Images were analyzed with ImageJ. To quantify chromocenters in *Drosophila*, 100 nuclei were counted in three brains per genotype and scored for the presence or absence of H3K9me2 or HP1α chromocenters. For quantification of experiments in control and JNPL3 mice, all motor neurons in spinal cord sections were counted and scored for the presence or absence of H3K9me2 or HP1α perinucleolar staining. For quantification of PIWIL1 immunostaining, ImageJ was used to measure PIWIL1 fluorescence intensity in motor neurons from at least five nonoverlapping microscopic fields at 40×.

Western blotting. Frozen *Drosophila* heads were homogenized in Laemmli sample buffer (Sigma), boiled for 10 min and analyzed by 15% SDS-PAGE (Lonza). Although whole heads contain a limited number of nuclei of non-nervous system origin, including epithelial- and muscle-derived nuclei, the simple external exoskeleton structure of the fly results in head preparations composed of primarily nervous system tissue. For western blots on neuronal nuclei from postmortem tissue, 150,000 sorted nuclei were loaded per lane. Full-length blots of the gels shown in the **Supplementary Figures** are provided in **Supplementary Figure 6**.

Locomotor behavioral assay. Flies were collected in fresh vials on the day of eclosion and were transferred without anesthesia to fresh vials on days 3, 5, 7 and 9. The locomoter assay was performed in the afternoon of day 10. To count the number of centimeters walked in 30 s, a single fly was tapped gently to the same initial starting position in its vial and the vial was placed over a gridded surface. The number of centimeters traversed was counted four times per fly, and 18 flies of each genotype were assayed.

Comet assay. Two brains per trial were dissected from adult flies in phosphate-buffered saline, homogenized with a plastic pestle and subjected to comet assay using commercially available reagents (CometAssay, Trevigen). 50 nuclei were quantified per trail using the ImageJ plugin Comet_Assay.

Chromatin immunoprecipitation and sequencing. Chromatin was prepared[51] and immunoprecipitated[52] as described with the following modifications. The heads of 2 g of male flies were ground in liquid nitrogen with a mortar and pestle before crosslinking with formaldehyde. Chromatin was sheared to 500 base pairs by 15 30-s bursts of sonication at 100% duty and level 5 power with a Branson Sonifier 450. IgG was used as a negative control. Libraries were prepared using the NEBNext ChIP-Seq Library Prep Reagent Set for Illumina according to the manufacturer's recommendations. DNA quality was measured at the Harvard Biopolymers Facility on an Agilent 2100 Bioanalyzer with a high sensitivity chip.

ChIP-seq analysis. Input and H3K9me2-ChIPped DNA was sequenced using an Illumina platform with a sequencing read length of 35 base pairs (Elim Biopharm). Experiments were carried out in biological duplicates. The number of reads for each experiment is summarized in **Supplementary Table 3**. Reads were aligned to the *Drosophila* genome using Bowtie[53] with the command

```
bowtie -tS -n 2 -l 28 -e 70 -p 1
dmel_genome.fasta file.txt file.sam
```

To identify genomic regions with reduced H3K9me2 levels in tau transgenic *Drosophila*, we developed a trough-finding algorithm. Conceptually, detecting a reduction in the amount of binding is similar to the widely studied problem of finding enriched regions, or peak calling.

As a pre-processing step, we first extended each read to 350 base pairs, as that was the average size of the ChIPped DNA fragment that was sequenced. The total read count was then normalized to 10,000,000 reads for each sample. Next, we subtracted the input from the ChIP for both tau and control experiments

$$\text{input\_normalized\_ChIP} = \text{ChIP} - \alpha \times \text{input}$$

where α is chosen such that the absolute value of the covariance between input and input_normalized_ChIP is minimized

$$\alpha = \arg\min \text{Cov}[\text{ChIP} - \alpha \times \text{input}, \text{input}]$$

This procedure ensures that the input is minimally informative about the normalized ChIP. We refer to these as the normalized, input-subtracted data, and we label them t and c for tau and control, respectively.

Next, we search for regions where t is significantly lower than c by scanning the genome with a window of size W base pairs that is moved using a step-size of w base pairs. For each window, we compare the number of reads in the two samples, and if the difference, $Z = c - t$, is larger than a critical value, z^*, the window is considered significant. To test whether a region is de-enriched, we used the null hypothesis that the normalized read counts for both tau and control follow normal distributions with mean and variance calculated based on the sample average and sample variance from all windows. The critical value, z^*, is determined using a false-discovery rate approach. Given that the distribution of reads is different for heterochromatic and euchromatic regions, we ran the algorithm for the two domains separately with different parameters for the null distribution. Euchromatic and heterochromatic regions were defined as by GenBank. Below is an outline of our algorithm in pseudo-code.

```
reduced_regions ← ∅
genes_affected ← ∅
for all windows w_i do
    z_i ← e_i − t_i
    if z_i < z* then
       add_item(reduced_regions, w_i)
       gene ← find_overlapping_gene(w_i)
       if gene ∉ ∅ then
          add_item(genes_affected, gene)
       end if
    end if
end for
```

The method add_item takes a list and an element as arguments and adds the element to the list if it is not already present. The method find_overlapping_gene takes a region of the *Drosophila* genome as input and returns the list of genes

where at least one base pair overlaps the region. If no genes overlap the region, the empty set is returned. Our final list used an FDR of 0.1, a window size of 1,000 base pairs and a step size of 100 base pairs. For the first experiment, we found 2,456 significant regions covering 167 different genes, and for the biological replicate we found 143 significant regions covering 22 different genes. There were 11 genes that were identified as significant in both experiments, and those were selected for further validation.

Quantitative PCR. H3K9me2 ChIP was performed on heads from 200 mg of whole *Drosophila* as described above. SYBR Green (Life Technologies) based qPCR was performed on an Applied Biosystems StepOnePlus Real-Time PCR System (**Supplementary Table 4**). For reverse transcription, RNA was extracted from ten *Drosophila* heads using QIAZOL (Qiagen) or from sorted NeuN-positive human neuronal nuclei. RNA concentrations were measured with a Nanodrop ND-1000 Spectrophotometer. Equal amounts of RNA were reverse transcribed using a cDNA Reverse Transcription Kit (Applied Biosystems), followed by qPCR (**Supplementary Table 4**). Each data point is the result of at least three biological replicates each composed of three technical replicates. *RpL32* is the internal control gene for *Drosophila* RT-PCR. *EIFA4* and *CYC1* were selected as internal controls for human RT-PCR based on their stability in postmortem brain of Alzheimer's disease patients[54]. Similar results were obtained with both internal controls.

Human brain analyses. For FACS analysis, human control and Alzheimer's disease brains with a postmortem interval of less than 24 h were collected through the autopsy service at Brigham and Women's Hospital under the appropriate IRB. Control brains included one male and five females, Braak stages I/II, with a median age of 70.5 and an age range of 65–80 years. Alzheimer's disease brains were from one male and five females, Braak stages V/VI, with a median age of 74.5 and an age range of 69–81 years. Nuclei were extracted and labeled with NeuN as described previously[55]. Nuclei were sorted at the Children's Hospital of Boston Flow Cytometry Research Facility on a BD Biosciences FACSAria Cell Sorter with BDFACS Diva software.

For large-scale expression analysis of human brain, we identified chromatin states as described in the main text. For blood, histone modifications in CD4+ cells were used to identify chromatin states. We used publicly available microarray data (GSE28146 (ref. 39), GSE16593 (ref. 56), GSE4226 (ref. 57)) and g:profiler[58] to map the microarray probes to genes. For genes with multiple probes, we calculated the geometric mean to associate one expression value with each gene. If the 5′ transcription start site of a gene overlapped one of the two heterochromatic states the gene was considered to be heterochromatic, otherwise it was considered to be euchromatic. For hippocampal neurons, 4,412 genes represented on the microarray were assigned to heterochromatin and 12,976 were assigned to euchromatin. For liver, 4,164 genes were assigned to heterochromatin and 13,214 were assigned to euchromatin. For blood, 1,474 genes were assigned to heterochromatin and 5,893 were assigned to euchromatin. Present/absent microarray calls were not available for the liver, so we set an arbitrary threshold and required that the mean of the $\log_2$ expression exceeded three in either sample.

Principal component analysis of gene expression from multiple brain samples. Using microarray data sets from hippocampal neurons from control and Alzheimer's disease brain, whole hippocampi of control brains and brains with different stages of Alzheimer's disease (GSE1297)[39], and whole fetal brain (GSE30803)[59], we defined heterochromatic genes as described above. Given that different array platforms were used for the samples, we only considered the 2,844 heterochromatic genes that were present on both platforms. To compare the expression levels between different samples, we first standardized the expression level for each sample by subtracting the mean and dividing by the s.d. We then calculated the principal components for the $g \times s$ matrix Y, where g represents the 2,844 genes and s represents the 7 different tissues. We next determined how the coefficients of the 'eigentissues' separated the different samples. We based similarity on whether each tissue was assigned a positive or negative coefficient for each principal component. The first component has positive coefficients for all samples, suggesting that it does not provide much relevant information. The second and third components group tissues from the same experiments, suggesting that a large degree of the variance is due to different experimental conditions. The first component that cannot be trivially explained by different experimental conditions is the fourth. It assigns Alzheimer's disease hippocampal neurons, severe Alzheimer's disease hippocampi, and fetal brains to the same category, suggesting that gene expression in these tissues is more similar than the other tissues.

Statistical analysis. All n values reported are biological replicates. No statistical methods were used to predetermine sample sizes, but our sample sizes are similar to those reported in previous publications[7,16,44]. For experiments in mice and human tissue, sample sizes were based on power analysis calculations, which demonstrated that a 30% difference between six cases and controls will achieve a power of 80%. Variance is similar between groups that are being compared. Data collection and analysis were not routinely performed blind to the conditions of the experiments. Data were collected and processed side by side in randomized order for all experiments. Data distribution was assumed to be normal, but this was not formally tested except for ChIP-seq analysis. Statistical analysis was performed using a one-way ANOVA when making multiple comparisons, and an unpaired Student's t test when making comparisons between two samples. The Wilcoxon rank-sum test was used for statistical analysis of RT-PCR from human NeuN-purified nuclei. This non-parametric test is the most appropriate to use when the underlying distribution is unknown and the sample size is small. The chi-square test was used for statistical analysis of microarray data. We tested for independence between both expression and chromatin states with a large sample size, and thus fulfilled the criteria for this non-parametric test.

51. Schwartz, Y.B. *et al.* Genome-wide analysis of Polycomb targets in *Drosophila melanogaster*. *Nat. Genet.* **38**, 700–705 (2006).
52. Gelbart, M.E., Larschan, E., Peng, S., Park, P.J. & Kuroda, M.I. *Drosophila* MSL complex globally acetylates H4K16 on the male X chromosome for dosage compensation. *Nat. Struct. Mol. Biol.* **16**, 825–832 (2009).
53. Langmead, B., Trapnell, C., Pop, M. & Salzberg, S.L. Ultrafast and memory-efficient alignment of short DNA sequences to the human genome. *Genome Biol.* **10**, R25 (2009).
54. Penna, I. *et al.* Selection of candidate housekeeping genes for normalization in human postmortem brain samples. *Int. J. Mol. Sci.* **12**, 5461–5470 (2011).
55. Jiang, Y., Matevossian, A., Huang, H.S., Straubhaar, J. & Akbarian, S. Isolation of neuronal chromatin from brain tissue. *BMC Neurosci.* **9**, 42 (2008).
56. Berzsenyi, M.D. *et al.* Down-regulation of intra-hepatic T-cell signaling associated with GB virus C in a HCV/HIV co-infected group with reduced liver disease. *J. Hepatol.* **55**, 536–544 (2011).
57. Maes, O.C. *et al.* Transcriptional profiling of Alzheimer blood mononuclear cells by microarray. *Neurobiol. Aging* **28**, 1795–1809 (2007).
58. Reimand, J., Kull, M., Peterson, H., Hansen, J. & Vilo, J. g:Profiler—a web-based toolset for functional profiling of gene lists from large-scale experiments. *Nucleic Acids Res.* **35**, W193–W200 (2007).
59. Martens, G.A. *et al.* Clusters of conserved beta cell marker genes for assessment of beta cell phenotype. *PLoS ONE* **6**, e24134 (2011).